An Improved Rotor Position Estimation With Vector-Tracking Observer in PMSM Drives With Low-Resolution Hall-Effect Sensors

Sam-Young Kim, *Member, IEEE*, Chinchul Choi, *Student Member, IEEE*, Kyeongjin Lee, and Wootaik Lee, *Member, IEEE*

***Abstract*—This paper presents an improved approach for estimating high-resolution rotor position in permanent-magnet synchronous motor (PMSM) drives with low-resolution Hall-effect sensors. A vector-tracking position observer in conjunction with discrete Hall sensors' output signals has been proposed, which is similar to a phase-locked loop structure. It consists of a position error detector, based on the vector cross product of the unit back-electromotive-force vectors obtained from a stator electrical model, and a proportional–integral-typed controller to make the position error rapidly converge to zero. This structure does not only compensate the misalignment effect of Hall sensors but also enhance their transient operating capability. The effectiveness of the proposed approach has been verified from several experiments in a low-voltage PMSM drive for automotive applications.**

***Index Terms*—Hall-effect sensors, high-resolution position estimation, permanent-magnet synchronous motor (PMSM), vector-tracking observer.**

I. Introduction

THE vector-controlled permanent-magnet synchronous motor (PMSM) drives are being increasingly used in a variety of high-performance applications such as aerospace, military, automotive, industrial, and household products. The proper vector-controlled operation absolutely depends on the accuracy of the rotor position information. Generally, this position information can be obtained from high-resolution sensors such as an incremental encoder or resolver mounted on a motor shaft. However, these sensors not only increase system cost, length, and size but also tend to reduce the system reliability [1]–[3]. In the case of employing the incremental encoder, an additional algorithm or procedure is necessary to obtain initial position at start-up.

Recently, various sensorless approaches have been developed as an alternative measure of shaft-mounted sensors, which are roughly categorized as methods based on back electromotive force (EMF) [3]–[6], flux linkage [7], [8], and rotor saliency [9], [10]. However, it is well known that most of the sensorless methods may not guarantee their performance in the entire speed and torque range [11]. In addition, these technologies have not been proven and matured to be practical for some mission-critical drives [12].

As a practical compromise, Hall sensors are often employed since they require little cost and volume compared with shaft-mounted sensors and provide discrete absolute-position information with electrically $\pm 30^\circ$ resolution. From discrete sensors' information, the high-resolution position can be estimated through some signal processing or error correction techniques.

In the last decades, several driving methods in the PMSM drives with Hall sensors have been proposed in the literature [1], [2], [13]–[17]. The techniques in [1] and [2] have used the discrete absolute position of $\pm 30^\circ$ resolution detected by a combination of three Hall signals at only start-up operation.

To estimate high-resolution rotor position from Hall signals, typical approaches based on average rotor speed have been presented such as the linear extrapolation technique [13] and the zeroth-order algorithm [14], [15]. In practice, these approaches may suffer from excessive average-speed error caused by intrinsic limitation—some assumptions that each Hall sensor is exactly aligned with stator magnetic axes, electrically 120° apart, and also the system operates at a constant speed.

Recently, some approaches to compensate the misalignment effect of Hall sensors have been introduced in [15]–[17]. The method in [15] has presented an automated process that can obtain the actual Hall state transition points in which an iterative routine determines the offset between ideal and actual points, and the resultant actual state transition values are stored in a lookup table during only initial commissioning. Since its main algorithm is based on the average speed, the performance may degrade at a variable-speed operation.

In [16], a vector-tracking observer using the vector-cross-product phase-detection method has been demonstrated, which uses the quantized rotating position vector at 60° obtained from Hall sensors' signals. In [17], an improved method of [16] is presented to decouple the intrinsic harmonic term in the quantized rotating position vector. These methods have zero-lag tracking capability. However, since the observer is based on the mechanical model of a machine, their position estimation may be easily affected by the system inertia and load variations.

Manuscript received April 23, 2010; revised July 23, 2010, October 1, 2010, and November 5, 2010; accepted November 17, 2010. Date of publication December 10, 2010; date of current version August 12, 2011.

S.-Y. Kim is with the Industrial-Academic Cooperation, Changwon National University, Changwon 641-773, Korea (e-mail: sam0kim@changwon.ac.kr).

C. Choi and K. Lee are with the Graduate School of Control and Instrumentation Engineering, Changwon National University, Changwon 641-773, Korea (e-mail: startchrap@changwon.ac.kr; jin4-8@changwon.ac.kr).

W. Lee is with the Department of Control and Instrumentation Engineering, Changwon National University, Changwon 641-773, Korea (e-mail: wootaik@changwon.ac.kr).

Color versions of one or more of the figures in this paper are available online at http://ieeexplore.ieee.org.

Digital Object Identifier 10.1109/TIE.2010.2098367

In this paper, a vector-tracking observer with a feedforward input of the average rotor speed is developed to derive the high-resolution rotor position. The basic structure of the observer is similar to a vector-tracking phase-locked loop (PLL), which consists of a phase detector based on vector cross product and a proportional–integral (PI) controller as a loop filter. The phase detector extracts the position estimation error, i.e., the phase difference between the reference unit back-EMF vector derived from a reference stator electrical model and the estimated unit back-EMF vector. Then, the PI controller makes the position error converge to zero rapidly, and it also appropriately corrects the feedforwarded average speed, including intrinsic errors caused by sensors' misalignments or speed variation. In addition, the feedforward input provides enough high-speed operating capability above the observer bandwidth. The proposed approach has been implemented on 16-b fixed-point DSP 56F8367 and evaluated through several experiments in a low-voltage PMSM drive for automotive applications.

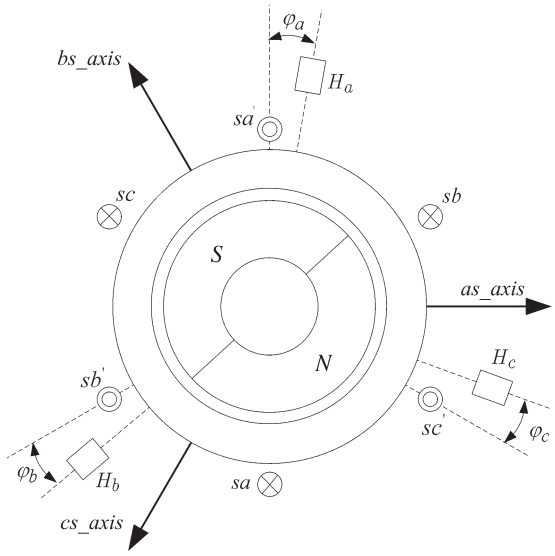

Fig. 1. Two-pole machine with misaligned Hall-effect sensors.

II. Rotor Position Estimation

In the PMSM drives with low-resolution Hall sensors, the absolute rotor position information with a resolution of $\pm 30^\circ$ can be obtained from the Hall sensors' signals. However, it is necessary that the resolution should be enhanced for achieving high-performance vector control.

A. Position Estimation With Average Rotor Speed

The high-resolution rotor position can be easily estimated through a method based on average rotor speed [13]–[16], where the six sectors are classified according to the states of the Hall sensor's signals. Assuming that the rotor speed within a sector is constant and the average speed in a current and previous sector is uniform, the rotor speed can be approximated as follows:

$$\omega_h = \frac{\frac{\pi}{3}}{\Delta t} \tag{1}$$

where Δt is the time interval of the previous sector. Then, the rotor position is estimated by the following numerical integration:

$$\widehat{\theta}_r = \theta_s + n \cdot \omega_h \cdot T_s \tag{2}$$

where θ_s is the measured absolute position in the current sector, n is the number of integration steps during the time interval of the current sector, and T_s is the sampling time. The rotor position $\widehat{\theta}_r$ satisfies $\theta_s \le \widehat{\theta}_r \le \theta_s + (\pi/3)$.

If the Hall sensors are symmetrically aligned in the motor, the rotor position obtained from (2) may be considerably precise value at the steady-state operation. However, since variable-speed operation or sensors' misalignment may cause an excessive average-speed error due to the aforementioned intrinsic limitation, the estimation error inevitably appears in practice and causes some performance degradation such as current distortions and torque pulsation.

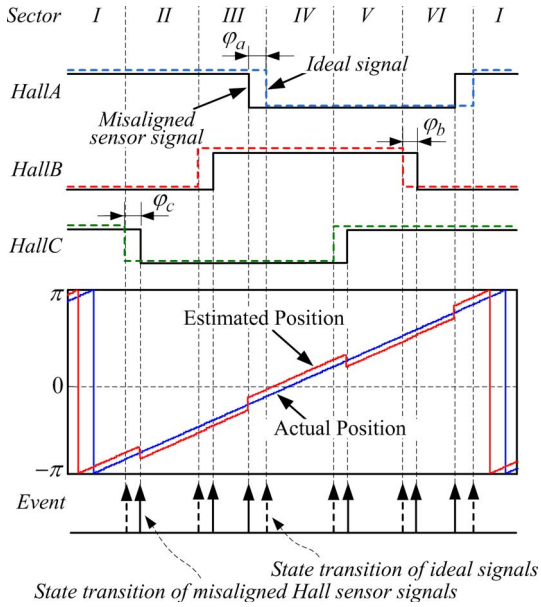

Fig. 2. Output signals of the misaligned Hall sensors and resultant position estimate.

A two-pole machine with misaligned Hall sensors is shown in Fig. 1, where φ_a, φ_b, and φ_c denote the angle differences between the actual stator magnetic axes and the practical placements of the corresponding Hall sensors. For instance, if the angle differences φ_a, φ_b, and φ_c are -15, 10, and 10 electrical degrees, respectively, the Hall sensor output signals and the resultant position estimate of (2) are shown in Fig. 2. In this figure, the rotor position is transiently distorted at each state transition of the misaligned Hall sensors' signals. Although it is not identified in Fig. 2, the speed transient operation such as start-up, speed, and load change may also raise the position estimation error in the method by (1) and (2) in practice since each sector's average speed may transiently change according to instantaneous or gradual change of the operating speed.

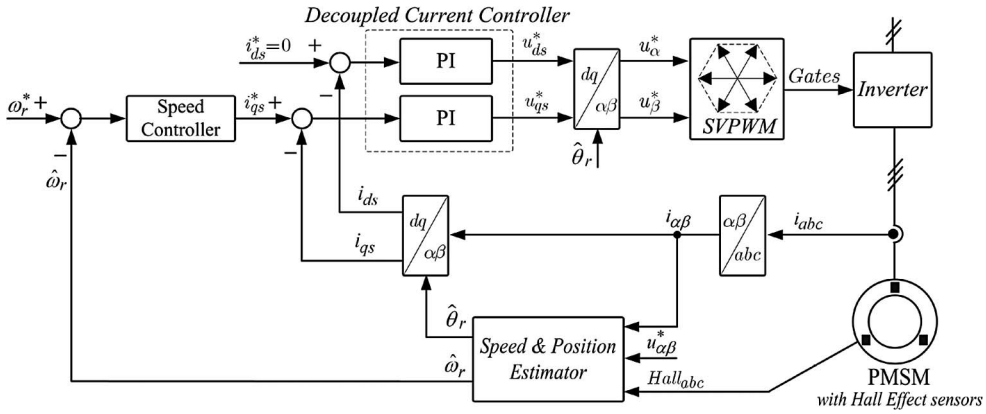

Fig. 3. Overall control scheme of the PMSM drive with Hall-effect sensors.

B. Proposed Vector-Tracking Position Estimation

To enhance the performance of the method based on average rotor speed, a vector-tracking position observer with a feedforward average-speed input is developed in this paper, which has a similar structure of a vector-tracking PLL as referred in [15]–[17] and is based on a reference stator electrical model.

In the case of the PMSM vector drives with Hall sensors, the general speed and decoupled current control loop in the synchronous reference frame with the position and speed estimator can be configured as shown in Fig. 3. The model equation in the stationary reference frame can be derived as follows:

$$\begin{bmatrix} u_\alpha^* \\ u_\beta^* \end{bmatrix} = \begin{bmatrix} R_s + pL_s & 0 \\ 0 & R_s + pL_s \end{bmatrix} \begin{bmatrix} i_\alpha \\ i_\beta \end{bmatrix} + \hat{\omega}_r \lambda_m \begin{bmatrix} -\sin\widehat{\theta}_r \\ \cos\widehat{\theta}_r \end{bmatrix} \tag{3}$$

$$\hat{\omega}_r = \omega_h + \omega_{\text{corr}} \tag{4}$$

where $u_{\alpha\beta}^*$ and $i_{\alpha\beta}$ represent the reference stator voltages and the measured stator currents, respectively. p is a derivative operator. R_s, L_s, and λ_m denote the stator resistance, the stator inductance, and the rotor flux linkage, respectively. $\hat{\omega}_r$ is the estimated rotor angular speed, including the average rotor speed ω_h, which is feedforwardly added to the proposed observer. ω_{corr} represents speed correction for the intrinsic error in ω_h.

Considering a digital control system with enough high sampling frequency, (3) can be expressed in discrete form. If the estimated rotor position, speed, and model parameters are the same as the actual values, the following equation can be obtained:

$$\begin{bmatrix} (u_\alpha^* - R_s i_\alpha) - L_s \frac{i_\alpha(k) - i_\alpha(k-1)}{T_s} \\ \left(u_\beta^* - R_s i_\beta\right) - L_s \frac{i_\beta(k) - i_\beta(k-1)}{T_s} \end{bmatrix} = \hat{\omega}_r \lambda_m \begin{bmatrix} -\sin\widehat{\theta}_r \\ \cos\widehat{\theta}_r \end{bmatrix} \tag{5}$$

where k is the sampling instant. The right side of (5) represents the estimate $\widehat{\overline{E}}$ of the back EMF established by the permanent magnet of the rotor. The left side represents the reference back EMF $\overline{E}^*$ calculated from the stator electrical circuits, where $\overline{E}^*$ can be filtered through a programmable low-pass filter (LPF), as represented in [18], to minimize the noise component without gain loss and phase delay. Then, the filtered reference back-EMF vector is represented as

$$\overline{E}_f^* = \frac{\overline{E}^*}{\tau s + 1}(1 + j\tau\hat{\omega}_r) \tag{6}$$

where τ is the time constant, which can be adjusted to the rotor speed $\hat{\omega}_r$.

The reference unit back EMF of $\overline{E}^*$ can be obtained as

$$\overline{e}^* = \frac{\overline{E}_f^*}{\left|\overline{E}_f^*\right|} = \begin{bmatrix} -\sin\theta_r^* \\ \cos\theta_r^* \end{bmatrix} \tag{7}$$

where θ_r^* is the phase angle of $\overline{e}^*$, which reflects the actual rotor position. Meanwhile, the estimated unit back EMF of $\widehat{\overline{E}}$ is equal to $\widehat{\overline{e}} = [-\sin\widehat{\theta}_r \ \cos\widehat{\theta}_r]^T$, which can be directly calculated from the estimated rotor position.

If the estimated rotor position and speed are the same as the actual values, $\overline{e}^*$ and $\hat{\overline{e}}$ are in-phase with each other. However, these may be out of phase in practice due to the estimation errors of speed/position and the parameter mismatches. Assuming that the difference of θ_r^* and $\widehat{\theta}_r$ is reasonably small, the position estimation error can be approximately detected from the following cross product of the unit back-EMF vectors $\overline{e}^*$ and $\hat{\overline{e}}$:

$$\begin{aligned} \|\overline{e}^* \times \widehat{\overline{e}}\| &= -\sin\theta_r^* \cos\widehat{\theta}_r + \cos\theta_r^* \sin\widehat{\theta}_r \\ &= \sin\left(\widehat{\theta}_r - \theta_r^*\right) \simeq -\theta_{\text{err}} \end{aligned} \tag{8}$$

where θ_{err} $(= \theta_r^* - \widehat{\theta}_r)$ is the position estimation error. Then, the speed correction ω_{corr} shown in (4) can be obtained by the following PI-typed controller as a loop filter of the proposed estimator so that the resultant value of (8) becomes zero:

$$\omega_{\text{corr}} = -\left(k_p + \frac{k_i \cdot T_s}{1 + z^{-1}}\right) \cdot \left[\|\overline{e}^* \times \widehat{\overline{e}}\| \cdot \text{sgn}(\widehat{\omega}_r)\right] \tag{9}$$

where the sign function $\text{sgn}(\widehat{\omega}_r)$ is to reflect the rotating direction of the rotor. k_p and k_i represent the proportional and integral gains, respectively.

In (9), ω_{corr} represents a speed correction corresponding to the position estimation error, i.e., the phase difference between the reference and estimated unit back-EMF vectors. From (4), the average rotor speed ω_h, including the intrinsic speed error, is appropriately corrected, and then, the estimated rotor speed $\hat{\omega}_r$ is converged to the actual rotor speed. Therefore, the high-resolution rotor position can be estimated by the following simple integration:

$$\widehat{\theta}_r(k) = \widehat{\theta}_r(k-1) + T_s\widehat{\omega}_r(k) \tag{10}$$

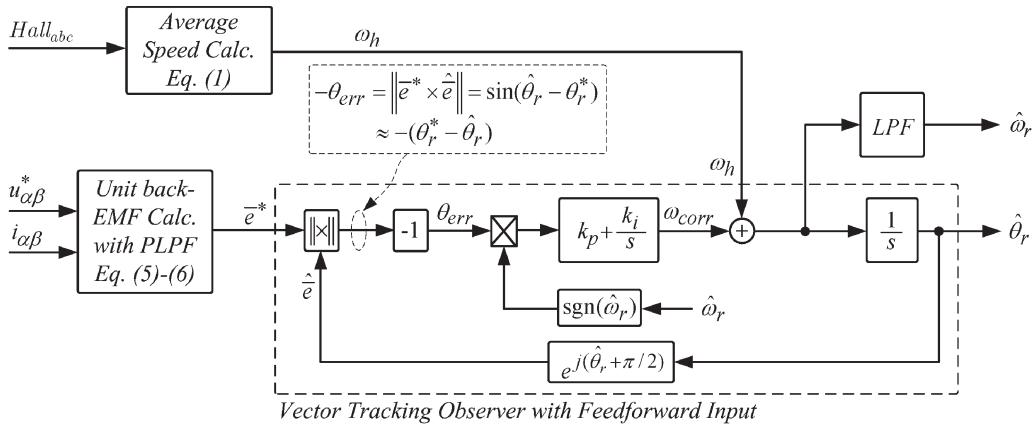

Fig. 4. Proposed vector-tracking position observer.

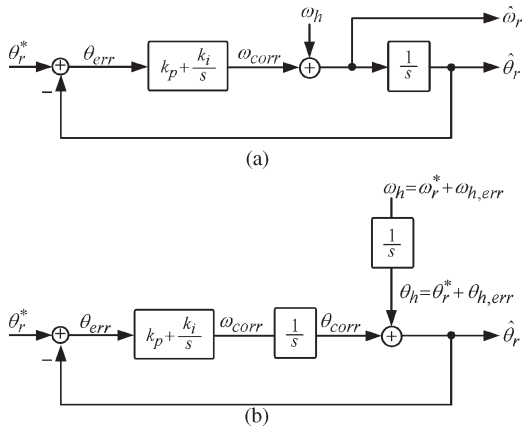

Fig. 5. Equivalent linear model of the vector-tracking observer with feedforward input. (a) Equivalent linear model. (b) Equivalent model of (a).

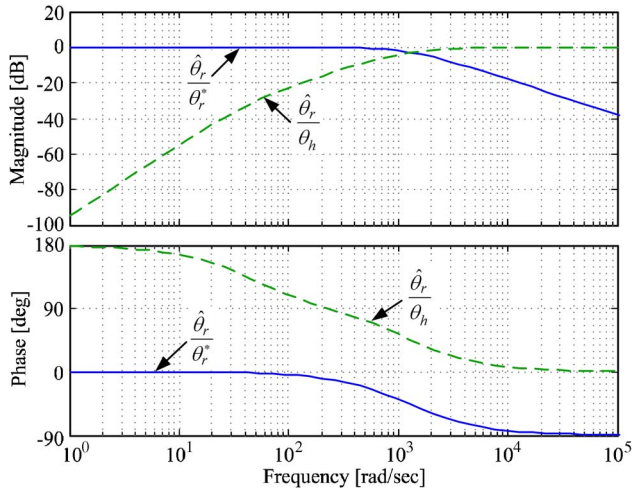

Fig. 6. Frequency response of the proposed observer ($k_p = 1268$ and $k_i = 54\,289$).

where k is the sampling instant. $\widehat{\theta}_r$ is initialized to the position with a resolution of $\pm 30^\circ$ obtained from the Hall sensors' signals at zero speed.

Although the speed correction algorithm of (9) cannot operate properly at and around zero speed, the proposed algorithm will provide useful position information by initializing the position state at zero speed and using the average speed ω_h in the estimated speed of (4).

C. Performance Evaluation of the Proposed Approach

The proposed vector-tracking position estimator described in (7)–(10) is shown in Fig. 4. In practical use, the estimated speed $\hat{\omega}_r$ has to be filtered through an LPF to enhance the noise immunity as shown in Fig. 4. The vector-tracking observer loop with feedforward input for the average speed ω_h can be equivalently transformed to a second-order linear model as shown in Fig. 5. From Fig. 5(b), the transfer function for the estimated position can be derived as

$$\widehat{\theta}_r = \frac{k_p s + k_i}{s^2 + k_p s + k_i}\theta_r^* + \frac{s^2}{s^2 + k_p s + k_i}\theta_h \qquad (11)$$

where θ_h represents the corresponding position to the average speed ω_h, which depicts the position feedforward input from the Hall sensors' signals.

From (11), it can be seen that the estimated position has the combined characteristics of the typical vector-tracking observation of reference position and the high-pass filtering of position feedforward input. Fig. 6 shows the frequency response of (11). In a real system, due to the intrinsic limitation of (1) for the average speed, the intrinsic error of position feedforward θ_h increases at a lower operating speed range, particularly initial start-up with maximally $\pm 30^\circ$ resolution in electrical angle. As shown in Fig. 6, the vector-tracking observer plays a key role in determining the characteristic of the entire observer loop at a lower speed range. That is, the observer appropriately corrects the intrinsic error of θ_h and estimates the actual position with zero-lag capability. On the contrary, at a high-speed range above the observer bandwidth, although the observer performance is certainly degraded, it is seen that the position feedforward input makes it possible to keep the zero-lag capability of the entire loop.

Considering that the average rotor speed ω_h consists of the actual rotor speed component ω_r^* and the intrinsic speed error $\omega_{h,\mathrm{err}}$, i.e., $\omega_h = \omega_r^* + \omega_{h,\mathrm{err}}$, as shown in Fig. 5(b), the loop output $\widehat{\theta}_r$ can be derived as $\widehat{\theta}_r = \theta_r^* + \theta_{h,\mathrm{err}} + \theta_{\mathrm{corr}}$, where $\theta_{h,\mathrm{err}}$ and θ_{corr} represent the corresponding positions to $\omega_{h,\mathrm{err}}$ and ω_{corr}, respectively. Therefore, the closed-loop

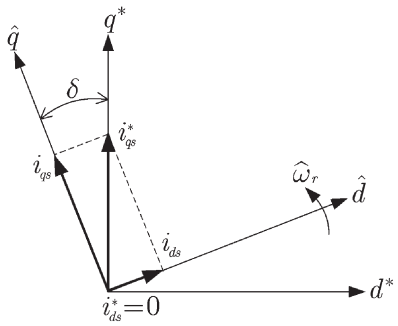

Fig. 7. Current vector diagram and load angle in the reference and estimation synchronous frames.

transfer function from the intrinsic position error $\theta_{h,\mathrm{err}}$ to its correction θ_{corr} is given as

$$\frac{\theta_{\mathrm{corr}}}{\theta_{h,\mathrm{err}}} = \frac{k_p s + k_i}{s^2 + k_p s + k_i} \tag{12}$$

where k_p and k_i are the proportional and integral gains of the PI controller, respectively. The estimating performance of $\widehat{\theta}_r$ relies on the dynamic performance of (12) determined by the design of only PI gains k_p and k_i. As represented in [3] and [19], the PI gains can be determined by $k_p = 2\zeta_n\omega_n$ and $k_i = \omega_n^2$ depending on the requirement of the correction/estimation speed and error tolerance, where ω_n and ζ_n are the natural frequency and the damping ratio in (12), respectively.

D. Improvement in the Load Change Condition

In pulsewidth-modulation (PWM) voltage-source inverter drives, the errors between the reference voltages and actual voltages of the machine tend to increase as the motor load increases due to the inverter nonlinearity effects [20], [21]. In (5) and (6), it is shown that the reference voltages, instead of the actual voltages, are used to estimate the back-EMF vector. Therefore, the back-EMF estimation error increases according to the motor load. This leads to an error in the speed correction ω_{corr} by (9) and then causes an error in the position estimate $\widehat{\theta}_r$ inevitably.

The instantaneous load torques can be used to compensate this error, where the load torques can be calculated in the reference and estimated synchronous frames shown in Fig. 7. The reference and estimated torques T_e^* and $\widehat{T}_e$ are respectively represented as

$$T_e^* = K_T i_{qs}^* \tag{13}$$

$$\widehat{T}_e = K_T i_{qs} \tag{14}$$

where K_T is the torque constant. i_{qs}^* represents the reference q-axis current generated by the speed controller. i_{qs} implies the estimated q-axis current, which is the transformed value with respect to the estimated position, i.e., $i_{qs} = i_\beta \cos\widehat{\theta}_r - i_\alpha \sin\widehat{\theta}_r$.

TABLE I
ROTOR ANGLE DISCREPANCY CAUSED BY MISALIGNED HALL SENSORS

Sector No.	Rotor angle discrepancy [deg] ($\Delta\theta = \theta_{ideal} - \theta_{meas}$)
I	-1.2
II	-3.0
III	7.2
IV	-3.3
V	0.6
VI	5.6

TABLE II
RATINGS AND PARAMETERS OF THE PMSM

Voltage	24 [V]
Current (peak)	8 [A]
Speed	3000 [rpm]
Torque	0.476 [N·m]
Stator resistance	0.158 [Ω]
Stator inductance	0.176 [mH]
Rotor flux linkage	6.55 [mWb]
Number of pole pairs	6

As can be seen in Fig. 7, if the load angle δ, which implies the position error induced by the motor load, is a very small value, (13) can be transformed as

$$\begin{aligned} T_e^* &= K_T(i_{ds}\sin\delta + i_{qs}\cos\delta) \\ &\simeq K_T(i_{ds}\delta + i_{qs}) \end{aligned} \tag{15}$$

where i_{ds} $(= i_\alpha \cos\widehat{\theta}_r + i_\beta \sin\widehat{\theta}_r)$ represents the estimated d-axis current.

From (14) and (15), the instantaneous torque error is given as

$$T_e^* - \widehat{T}_e = K_T i_{ds}\delta. \tag{16}$$

Therefore

$$i_{ds}\delta = i_{qs}^* - i_{qs}. \tag{17}$$

In (17), it is clear that the right side $(i_{qs}^* - i_{qs})$ reflects the information of the load angle δ. Therefore, the load angle can be estimated by the following PI-typed controller:

$$\widehat{\delta} = \left(k_{pc} + \frac{k_{ic}\cdot T_s}{1+z^{-1}}\right)(i_{qs}^* - i_{qs}) \tag{18}$$

where $\widehat{\delta}$ is the estimated load angle. k_{pc} and k_{ic} are the proportional and integral gains, respectively.

The total position estimation error can be considered as the sum of the position error of (8) and the estimated load angle of (18). As in (19), if the estimated load angle of (18) is added to the speed correction of (9), the proposed vector-tracking observer may enhance the position estimation performance by correcting the load-induced error

$$\omega_{\mathrm{corr}} = -\left(k_p + \frac{k_i\cdot T_s}{1+z^{-1}}\right)\cdot\left[\|\overline{e}^* \times \widehat{\overline{e}}\|\cdot \mathrm{sgn}(\widehat{\omega}_r) - \widehat{\delta}\right]. \tag{19}$$

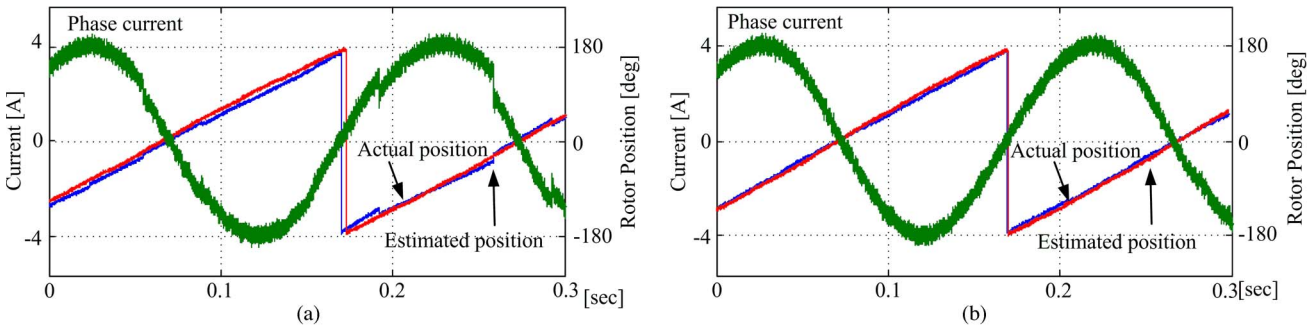

Fig. 8. Stator current waveform and rotor position at steady-state 50 r/min. (a) With the average-speed-based approach. (b) With the proposed approach.

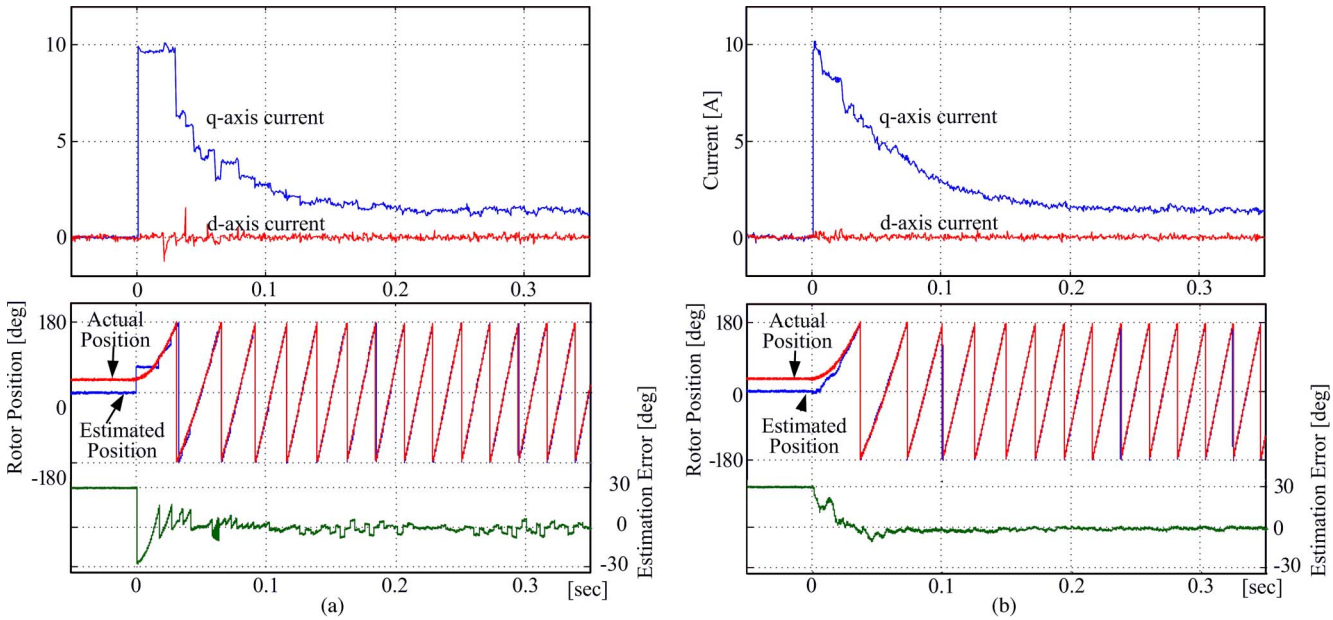

Fig. 9. Start-up 0 to 500 r/min. (a) With the average-speed-based approach. (b) With the proposed approach.

III. Experimental Results

Several experiments have been performed to validate the proposed vector-tracking position estimator. In the experiments, the characteristics of the proposed approach have been presented through a comparative study with the results of the average-speed-based approach.

The overall control scheme of the experimental drive is shown in Fig. 3, which has been implemented on 16-b fixed-point DSP 56F8367. The PWM frequency of the inverter is set to 16 kHz. The current control and the proposed vector-tracking position observer loop are synchronously executed with PWM period. The test motor is a low-voltage surface-mounted PMSM for an automotive application, which employs three Hall sensors misaligned with the stator magnetic axes. Each angle difference in actual sensor placements, i.e., φ_a, φ_b, and φ_c, has been measured as about 5.6, -3.0, and 3.3 electrical degrees, respectively. Table I shows the angle discrepancies of the measured absolute position in each sector caused by these misplacements. An incremental encoder with a resolution of 3600 pulses/rev has been mounted on the shaft of the test bench for comparison between the estimated position $\widehat{\theta}_r$ and the actual rotor position θ_r. Other specifications of the drive system are given in Table II. Fig. 8 shows the phase current waveforms, actual position, and estimated position at the steady-state operation of 50-r/min speed and 4-A load. In the result of the average-speed-based approach in Fig. 8(a), it can be seen that the current waveform is seriously distorted and the position is corrected abruptly at the end of every 60° sector. This is due to the combined effects caused by an average-speed error and the Hall sensors' misalignment. On the contrary, in the result of the proposed method in Fig. 8(b), it is shown that the waveform distortion is rarely found and the position is exactly corrected/estimated without an unacceptable estimation position error.

Fig. 9 shows the start-up response of the speed change from standstill to 500 r/min, where the initial position was intentionally set to about 30 electrical degrees—the maximum position error allowed in the system using the Hall sensors. With the average-speed-based approach in Fig. 9(a), although the magnitude of the position estimation error is limited within maximally ± 30 electrical degrees, the excessive estimation error transiently appears at the end of every 60° sector, and also, excessive ripples of d- and q-axis currents synchronously appear in accordance with the transient of the estimated position,

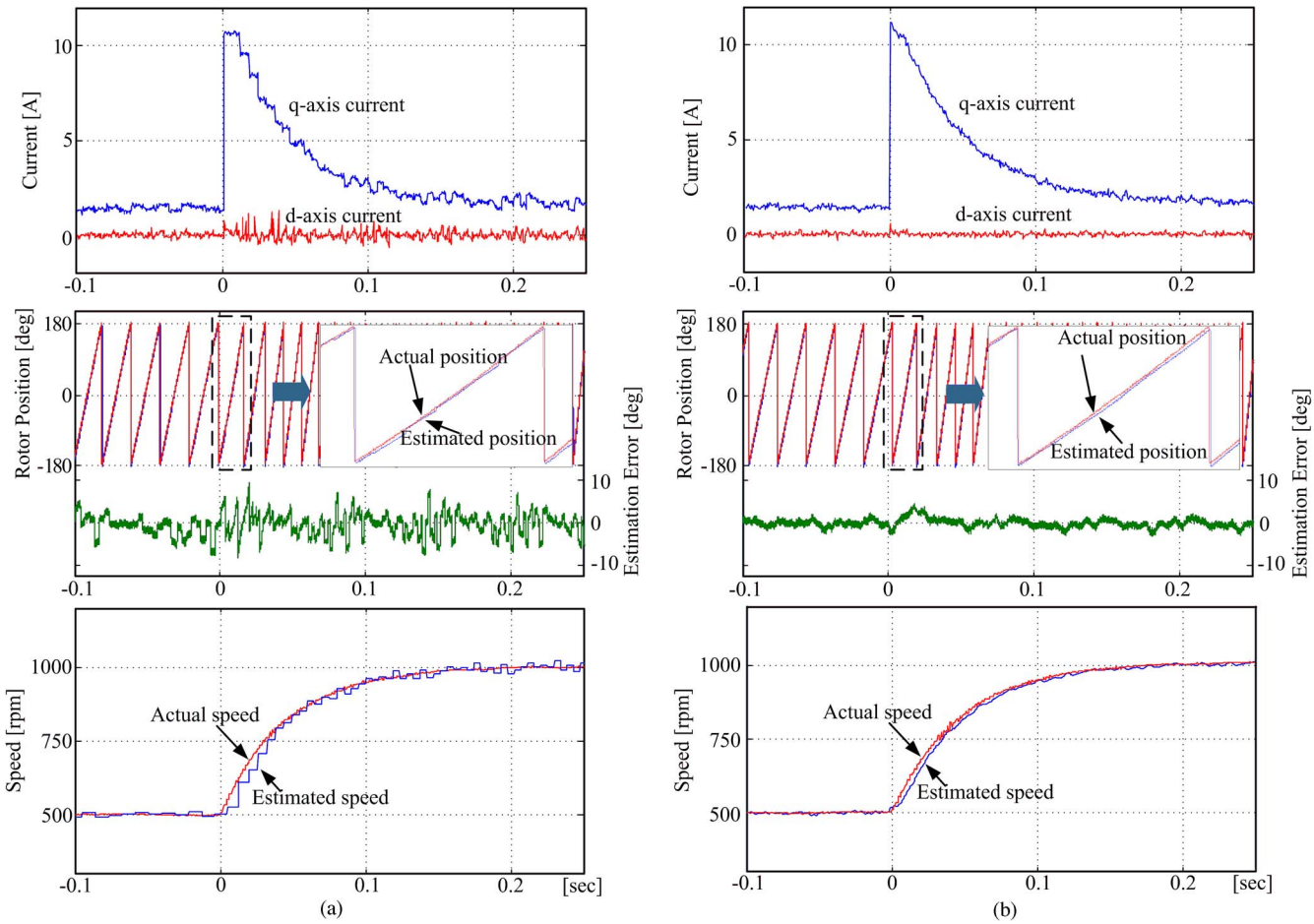

Fig. 10. Speed change from 500 to 1000 r/min at near no load. (a) With the average-speed-based approach. (b) With the proposed approach.

since the average-speed error excessively increases at the speed transient. However, with the proposed approach in Fig. 9(b), the estimation position error $(\theta_r - \widehat{\theta}_r)$ is rapidly corrected to zero from a limited initial position error, and also, a few d- and q-axis current ripples appear without transient changes compared with the average-speed-based approach in Fig. 9(a).

Figs. 10 and 11 show the step responses of the speed (from 500 to 1000 r/min at near no load) and load changes (from near-no-load to 4-A current at 500 r/min). With the average-speed-based approach in Figs. 10(a) and 11(a), it is clearly shown that, during the speed/load transient, as well as steady state, the transiently changing estimation position error and the estimated speed still appear at the end of every 60° sector even though they are relatively small compared to those of the start-up transient as shown in Fig. 9(a). On the contrary, with the proposed approach in Figs. 10(b) and 11(b), these errors are remarkably eliminated, and good dynamic performance of the proposed approach is confirmed.

Fig. 12 shows the load step response from near-no-load to full-load current at 500-r/min speed, where Fig. 12(a) and (b) shows the resulting waveforms without and with the load angle compensation algorithm of (18) and (19), respectively. When the full load is applied, the estimation error increases as much as the load angle (about ±1 electrical degree) without the compensation of Fig. 12(a). With the load angle compensation algorithm, this estimation error is eliminated in the steady state as shown in Fig. 12(b).

Fig. 13 shows the total harmonic distortions (THDs) of the stator phase current characterized under the different load current and speed conditions, where the THD for the presented purpose is defined as

$$\text{THD} = \sqrt{\sum_{n=2}^{20} I_n^2} \Big/ I_1 \tag{20}$$

where I_1 and I_n are the fundamental component and nth-order harmonic component of the stator current, respectively.

As can be seen in Fig. 13, the THD has been remarkably reduced in the result graph of the proposed approach compared to that of the average-speed-based approach even if there is some increasing tendency of THD at the higher speed range.

IV. Conclusion

In this paper, a vector-tracking position observer has been proposed to derive the high-resolution rotor position in the PMSM drives with low-resolution Hall sensors. The proposed approach has a similar PLL structure, which has the feedforward input for the average speed and is initialized to absolute

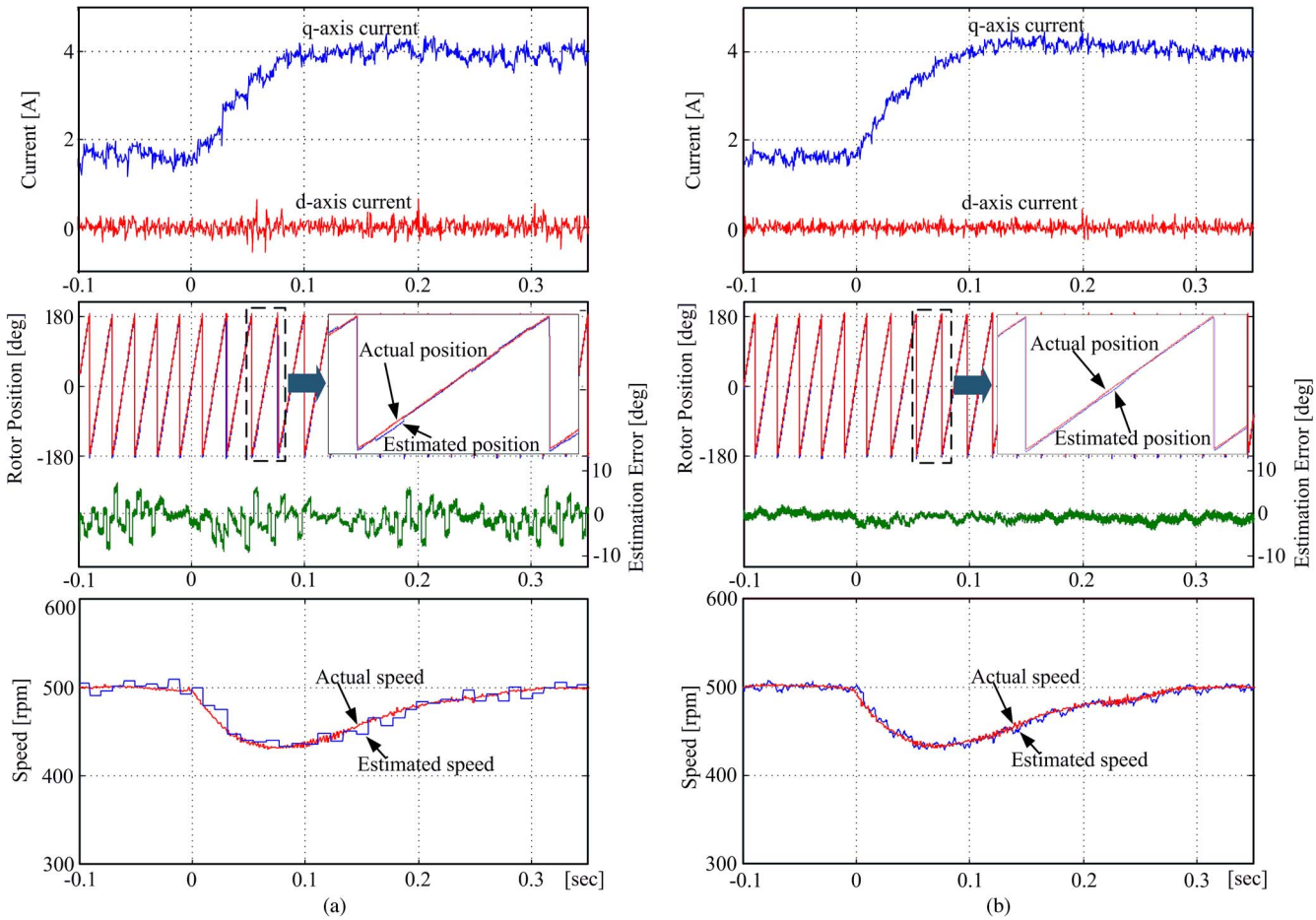

Fig. 11. Load change at 500 r/min. (a) With the average-speed-based approach. (b) With the proposed approach.

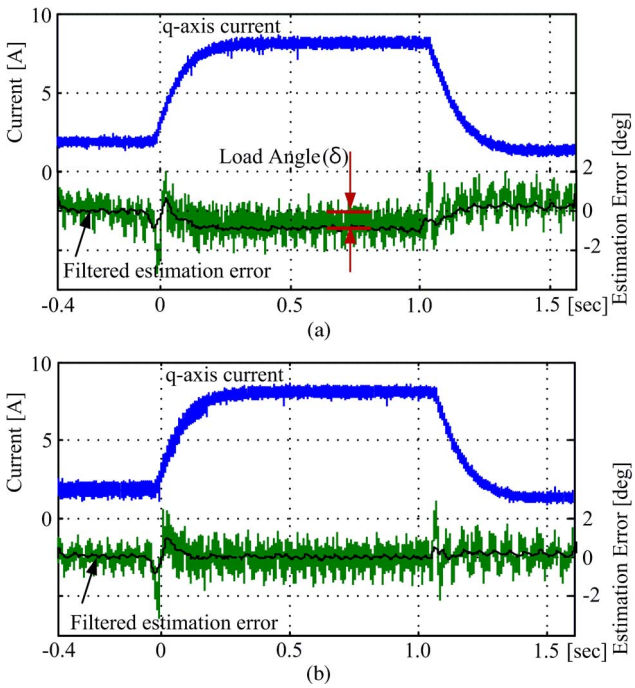

Fig. 12. Load step response at 500 r/min: (a) Without and (b) with the load angle compensation.

position with a resolution of ±30° obtained from the Hall sensors' output signals. This structure allows the proposed approach to provide useful position information even at and

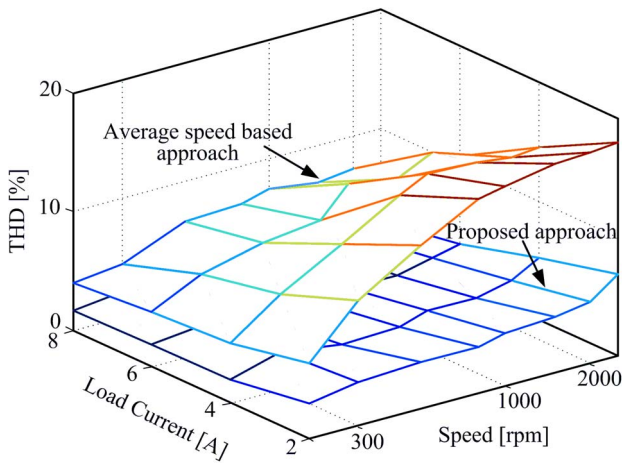

Fig. 13. THD analysis.

around zero speed where the vector-tracking correction loop cannot correctly operate. Above zero speed, the proposed approach provides the high-resolution position information, where the position estimation error rapidly converges to zero regardless of the misalignment of Hall sensors and the excessive average-speed error, particularly speed transient operation. Through the experiments at the steady-state, start-up, speed transient, and load transient operations, the effectiveness and the dynamic performance of the proposed approach have been evaluated and verified.

REFERENCES

[1] T. D. Batzel and K. Y. Lee, "Slotless permanent magnet synchronous motor operation without a high resolution rotor angle sensor," *IEEE Trans. Energy Convers.*, vol. 15, no. 4, pp. 366–371, Dec. 2000.

[2] A. Lidozzi, L. Solero, F. Crescimbini, and A. Di Napoli, "SVM PMSM drive with low resolution Hall-effect sensors," *IEEE Trans. Power Electron.*, vol. 22, no. 1, pp. 282–290, Jan. 2007.

[3] S. Morimoto, K. Kawamoto, M. Sanada, and Y. Takeda, "Sensorless control strategy for salient-pole PMSM based on extended EMF in rotating reference frame," *IEEE Trans. Ind. Appl.*, vol. 38, no. 4, pp. 1054–1061, Jul./Aug. 2002.

[4] Z. Chen, M. Tomita, S. Doki, and S. Okuma, "An extended electromotive force model for sensorless control of interior permanent-magnet synchronous motors," *IEEE Trans. Ind. Electron.*, vol. 50, no. 2, pp. 288–295, Apr. 2003.

[5] D. Cascadei, G. Serra, A. Stefani, A. Tani, and L. Zarri, "DTC drives for wide speed range applications using a robust flux-weakening algorithm," *IEEE Trans. Ind. Electron.*, vol. 54, no. 5, pp. 2451–2461, Oct. 2007.

[6] F. Genduso, R. Miceli, C. Rando, and G. R. Galluzzo, "Back EMF sensorless-control algorithm for high-dynamic performance PMSM," *IEEE Trans. Ind. Electron.*, vol. 57, no. 6, pp. 2092–2100, Jun. 2010.

[7] I. Boldea, M. C. Paicu, and G. D. Andreescu, "Active flux concept for motion sensorless unified ac drives," *IEEE Trans. Power Electron.*, vol. 23, no. 5, pp. 2612–2618, Sep. 2008.

[8] G. Foo and M. F. Rahman, "Sensorless direct torque and flux-controlled IPM synchronous motor drive at very low speed without signal injection," *IEEE Trans. Ind. Electron.*, vol. 57, no. 1, pp. 395–403, Jan. 2010.

[9] S. Y. Kim and I. J. Ha, "A new observer design method for HF signal injection sensorless control of IPMSMs," *IEEE Trans. Ind. Electron.*, vol. 55, no. 6, pp. 2525–2529, Jun. 2008.

[10] Q. Gao, G. M. Asher, M. Sumner, and L. Empringham, "Position estimation of a matrix-converter-fed AC PM machine form zero to high speed using PWM excitation," *IEEE Trans. Ind. Electron.*, vol. 56, no. 6, pp. 2030–2038, Jun. 2009.

[11] J. W. Finch and D. Giaouris, "Controlled AC electrical drives," *IEEE Trans. Ind. Electron.*, vol. 55, no. 2, pp. 481–491, Feb. 2008.

[12] A. Emadi, Y. J. Lee, and K. Rajashekara, "Power electronics and motor drives in electric, hybrid electric, and plug-in hybrid electric vehicles," *IEEE Trans. Ind. Electron.*, vol. 55, no. 6, pp. 2237–2245, Jun. 2008.

[13] B.-H. Bae, S.-K. Sul, J.-H. Kwon, and J.-S. Byeon, "Implementation of sensorless vector control for super-high-speed PMSM of turbocompressor," *IEEE Trans. Ind. Appl.*, vol. 39, no. 3, pp. 811–818, May/Jun. 2003.

[14] S. Morimoto, M. Sanada, and Y. Takeda, "High-performance current-sensorless drive for PMSM and SynRM with only low-resolution position sensor," *IEEE Trans. Ind. Appl.*, vol. 39, no. 3, pp. 792–801, May/Jun. 2003.

[15] B. B. Philip, D. P. Steven, J. D. Bradley, and C. K. Andreas, "Compensation for asymmetries and misalignment in a Hall-effect position observer used in PMSM torque-ripple control," *IEEE Trans. Ind. Appl.*, vol. 43, no. 2, pp. 560–570, Mar./Apr. 2007.

[16] F. Giulii Capponi, G. De Donato, L. Del Ferraro, O. Honorati, M. C. Harke, and R. D. Lorenz, "AC brushless drive with low-resolution Hall-effect sensors for surface-mounted PM machines," *IEEE Trans. Ind. Appl.*, vol. 42, no. 2, pp. 526–535, Mar./Apr. 2006.

[17] M. C. Harke, G. De Donato, F. Giulii Capponi, T. R. A. Tesch, and R. D. Lorenz, "Implementation issues and performance evaluation of sinusoidal, surface-mounted PM machine drives with Hall-effect position sensors and a vector-tracking observer," *IEEE Trans. Ind. Appl.*, vol. 44, no. 1, pp. 161–173, Jan./Feb. 2008.

[18] B. Karanayil, M. F. Rahman, and C. Grantham, "An implementation of a programmable cascaded low-pass filter for a rotor flux synthesizer for an induction motor drive," *IEEE Trans. Power Electron.*, vol. 19, no. 2, pp. 257–263, Mar. 2004.

[19] L. Idkhajine, E. Monmasson, M. W. Naouar, A. Prata, and K. Bouallaga, "Fully integrated FPGA-based controller for synchronous motor drive," *IEEE Trans. Ind. Electron.*, vol. 56, no. 10, pp. 4006–4017, Oct. 2009.

[20] S.-Y. Kim, W. Lee, M.-S. Rho, and S.-Y. Park, "Effective dead-time compensation using a simple vectorial disturbance estimator in PMSM drives," *IEEE Trans. Ind. Electron.*, vol. 57, no. 5, pp. 1609–1614, May 2010.

[21] R. J. Kerkman, D. Leggate, D. W. Schlegel, and C. Winterhalter, "Effects of parasitics on the control of voltage source inverters," *IEEE Trans. Ind. Electron.*, vol. 18, no. 1, pp. 140–150, Jan. 2003.

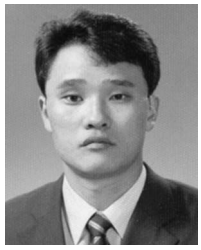

Sam-Young Kim (S'04–M'06) received the B.S., M.S., and Ph.D. degrees in electronic engineering from Changwon National University, Changwon, Korea, in 1997, 1999, and 2005, respectively.

From 1997 to 2003, he was with Doosan Heavy Industries and Construction Company, Ltd., Changwon, where he was a Senior Engineer for developing triple-modular-redundancy systems for generator excitation control systems. Since 2005, he has been a Research Professor with Industrial-Academic Cooperation, Changwon National University. His research interests include high-performance electrical machine drives, generator excitation control systems, and DSP-based applications.

Chinchul Choi (S'07) received the B.S. and M.S. degrees in control and instrumentation engineering from Changwon National University, Changwon, Korea, in 2006 and 2008, respectively, where he is currently working toward the Ph.D. degree in the Graduate School of Control and Instrumentation Engineering.

His research interests include the control, modeling, and fault diagnosis of electric drive systems.

Kyeongjin Lee received the B.S. and M.S. degrees in control and instrumentation engineering from Changwon National University, Changwon, Korea, in 2008 and 2010, respectively.

He is currently with the Graduate School of Control and Instrumentation Engineering, Changwon National University. His research interests include the software development of automotive electronic management systems.

Wootaik Lee (M'06) received the B.S. and M.S. degrees in electrical engineering and the Ph.D. degree in automotive engineering from Hanyang University, Seoul, Korea, in 1996, 1998, and 2002, respectively.

From 2001 to 2003, he was with the Automotive Control and Electronics Research Center, Seoul, where he was a Senior Engineer for developing automotive electronic control units and designing in-vehicle control networks. Since 2003, he has been with the Department of Control and Instrumentation Engineering, Changwon National University, Changwon, Korea, where he is currently an Assistant Professor. His research interests include model-based development processes for embedded control systems and motor drives for automotive applications.